Regeneration of Spent Bleaching Earth by Calcination and Its Morphological Enhancement via KOH Impregnation

Ika Kusuma Nugraheni[1*], Jaka Darma Jaya[1], Nuryati Nuryati[1], Sunardi Sunardi[2], Utami Irawati[2], Putri Iis Faiza[1], and Dita Adi Saputra[3]**

[1]*Department of Agroindustry, Tanah Laut State Polytechnic, Jl. A. Yani Km. 6, Pelaihari, Tanah Laut 70815, Indonesia*

[2]*Department of Chemistry, Lambung Mangkurat University, Jl. A. Yani Km. 36, Banjarbaru 70713, Indonesia*

[3]*Research Center for Fuel Technology, National Research and Innovation Agency (BRIN), KST BJ Habibie, Setu, Tangerang Selatan 15314, Indonesia*

Corresponding author:

tel: +62-85248129040; +62-8114000349***
email: ika.kusuma.n@politala.ac.id; sunardi@ulm.ac.id***

Received: September 1, 2024
Accepted: October 28, 2025

DOI: 10.22146/ijc.99600

Abstract: *Spent bleaching earth (SBE), a waste generated from palm oil bleaching, contains residual oil and organic matter that block its pore structure and pose environmental disposal concerns. Regeneration of SBE is therefore essential to enable its reutilization. In this study, SBE was regenerated by calcination and further modified via KOH impregnation at concentrations of 1.00, 0.10, and 0.01 M. The regenerated materials were characterized using XRF, SEM, TEM, XRD, and BET surface area analysis. Calcination combined with 0.10 M KOH impregnation increased the surface area from 8.70 to 93.81 m^2/g, approaching the value of activated bleaching earth (94.29 m^2/g), and significantly altered pore volume and pore size distribution. These findings indicate that calcination restores the basic structure of SBE, while subsequent KOH impregnation enhances its morphological properties, highlighting the potential of regenerated SBE as a low-cost adsorbent or catalyst support.*

Keywords: *SBE regeneration; KOH-impregnation; morphological characterization*

■ INTRODUCTION

Crude palm oil (CPO) is a variety of palm oil that goes through a refining process that includes filtration to remove impurities such as dirt and gum (degumming) [1]. Adsorbents are used to bleach the oil, which improves its look, taste, aroma, and stability [2]. The bleaching method utilizes an adsorbent derived from bentonite, a solid structure composed of montmorillonite that is chemically activated. Bleaching earth (BE) is a commonly used adsorbent in the bleaching process.

BE is a frequently used adsorbent due to its widespread availability and economic worth. BE can eliminate unwanted elements, such as oil pigmentation and heavy metals. BE will produce spent BE (SBE), a solid waste material resembling colored sand [3]. SBE, which exists in the refinery unit within a temperature range of 80–120 °C, can trigger oxidation reactions when it comes into contact with ambient oxygen. Due to its ability to undergo an oxidation reaction that produces sufficient heat to initiate fire and result in self-ignition, SBE is categorized as a material that can pose a fire danger [4].

BE is a clay material, commonly montmorillonite-based, that consists primarily of aluminosilicates (SiO_2 and Al_2O_3) [5] with minor oxides component such as Fe_2O_3, CaO, and MgO [6]. During the bleaching of CPO, the clay adsorbs pigments, phospholipids, free fatty acids (FFA), soaps, and other organic impurities. As a result, the SBE contains both the inorganic clay matrix and a significant fraction of residual organics (20–40 wt.%) [7], including triglycerides, oxidized fatty acids, and hydrocarbons, as well as trace metals derived from the oil or processing. The inorganic framework of SBE is thus composed mainly of amorphous and crystalline silica, alumina, and silicate phases, while its organic fraction makes it carbon-rich and thermally unstable.

On the other hand, the primary environmental consequence of SBE is soil and water pollution [8]. Improper disposal of substances containing dangerous chemical components, such as FFA, phenol, and heavy metals, can lead to a decline in soil and water quality [9]. SBE is classified as one of the eight types of waste that do not fall under the category of hazardous waste. Both oleochemical industrial processes and the processing of animal and vegetable oils employ SBE. The classification of this material as waste necessitates the application of the reutilization process [10].

Several techniques have been employed to recycle SBE, including thermal, chemical, and solvent extraction approaches. The thermal treatment exposes the substance SBE to calcination, heating it to 350 °C for 1 h. Subsequently, a 1 M HCl solution is employed to wash the material, aiming to bleach it and reduce the oil peroxide value [11]. The addition of HCl, HNO_3, or H_2SO_4 causes the chemical regeneration of SBE. Furthermore, solvent extraction using *n*-hexane, acetone, and methyl ethyl ketone [2] can be used to purify SBE. However, using acids can produce dangerous fumes that endanger both the equipment and the workers engaged in the oil production process. Consuming processed oil containing acid levels beyond a specific threshold has the potential to cause cancer and subsequent liver and stomach disorders [12]. Consequently, acids are excluded from the process of preparing SBE for food products. Furthermore, using solvents in SBE regeneration has several disadvantages, including increased energy consumption, the extraction of vital components, and the requirement for water in the purification process [13]. Moreover, solvents possess the capacity to damage the environment.

For SBE pretreatment, an acid-free and solvent-free approach involves exposing the material to a temperature of 587 °C for 108 min. This process produces SBE with comparable characteristics to activated BE, making it suitable for bleaching soybean oil [14]. Furthermore, the alkaline impregnation technique can effectively convert SBE into a silica adsorbent. NaOH, an alkaline compound, may effectively erode the inner surfaces of clay minerals, leading to a system with a significant surface area of 100 $m^2 g^{-1}$ and a total pore volume of 0.3 $cm^3 g^{-1}$ [15]. The best results for SBE uptake of fluoride ions are achieved through impregnation with a NaOH solution. The addition of alkali alters the tetrahedral layer. This modifies the physical and chemical properties of the pores, particularly their ability to exchange cations, altering the SBE's capacity to retain molecules [16].

Previous studies have demonstrated that impregnation with KOH can effectively modify zeolite catalysts for biodiesel production from palm oil mill effluent. However, research on the regeneration of SBE using alkaline modification remains limited. To date, no systematic study has reported the use of KOH for enhancing the morphological properties of regenerated SBE. While calcination is widely applied for SBE regeneration, its combination with alkali treatment, particularly KOH impregnation, has not been fully explored. Therefore, this study aims to investigate the morphological and structural characteristics of KOH-impregnated SBE regenerated by calcination, using SEM, TEM, XRD, and pore size analysis.

■ EXPERIMENTAL SECTION

Materials

The material used in this study are from CPO refinery factory in South Kalimantan, Indonesia. Chemicals of KOH with pro-analytical analysis quality were purchased from Merck, Germany. Distilled water was obtained from CV. Delta Surya, Banjarmasin, which is used as a solvent in generating KOH solution.

Instrumentation

The experimental instruments in this study include scanning electron microscope (SEM, HITACHI SU3500/JEOL JSM-IT200), transmission electron microscope (TEM, TALOS F200C G2), X-ray diffraction (XRD, Aeris PANalytical instrument), and Brunauer Emmett Teller (BET) surface area & pore size distribution (Quantachrome Instruments).

Procedure

SBE preparation

SBE was treated using a hot water washing process. A 10% (w/v) suspension of SBE was heated to 100 °C with agitation for 20 min. The solid was then separated by

decantation, followed by vacuum filtration using a filter with a pore size of 2.5 μm. The SBE was obtained by drying it at 105 °C until it reached a fine powder consistency.

Thermal regeneration of SBE

A 5 g of SBE were exactly introduced into the furnace, which was heated to 587 °C for 108 min. The regeneration time is deemed to commence once the test temperature of 12 °C is reached.

SBE impregnation by KOH

KOH solutions with concentrations of 0.01, 0.10, and 1.00 M were prepared using deionized water as the solvent. Calcined SBE was added to the KOH solution at various concentrations, with each mixture containing 10% (w/w) SBE relative to KOH. After soaking for 24 h, the samples were placed in an oven (105 °C; 24 h). The samples were then heated for an additional 2 h to stabilize the KOH interaction in SBE. Then, the samples were rinsed with a 2 M HCl solution and deionized water until they were neutral. Finally, the samples were dried at 80 °C for 24 h. After that, the regenerated SBE was meshed into powder and filtered using filter paper. This impregnated SBE is referred to as K-SBE. In this study, several variations of sample treatment with different concentrations were conducted to determine the optimal characteristics of the adsorbent, which are listed in Table 1.

Characterization of K-impregnated SBE

The morphology of the materials was characterized using SEM and TEM to examine SBE, SBE after thermal treatment, SBE impregnated with KOH, and BE. In SEM analysis, carbon-coated samples were prepared and analyzed using a JEOL JFC 1100 sputter. In addition to providing information about the condition of the adsorbent surface, the SEM analysis results also revealed the distribution of metal oxides scattered on the surface.

Table 1. Sample variations

Sample	Description
SBE	Spent bleaching earth
SBE-T	SBE thermal
K-SBE-1	SBE impregnation by KOH (1.00 M)
K-SBE-0.1	SBE impregnation by KOH (0.10 M)
K-SBE-0.01	SBE impregnation by KOH (0.01 M)
BE	Bleaching earth as a comparison

TEM analysis was performed using an HRTEM Talos F200C G2 instrument.

Crystallinity and structure of catalysts were analyzed using XRD. The crystalline phase analysis was performed using an Aeris PANalytical XRD system with a Cu anode, at a scan speed of 0.0167 s per step. Measurement of 2θ distance was carried out at 7–90°. The BET method was used to measure the surface area of SBE, SBE after treatments, and SBE impregnation by KOH. The surface area analyzer (SAA) device used a 300 °C degassing temperature to examine the surface area and pore properties of each material [17]. Using the BET technique, the specific surface area and total pore volume were calculated through a surface area analyzer [18]. Pore size estimation was also conducted using the Barrett-Joyner-Halenda (BJH) method. The BET test is used to ascertain the material's surface area, pore distribution, and SBE pore volume.

■ RESULTS AND DISCUSSION

Component Analysis of BE and SBE

The X-ray fluorescence (XRF) analysis revealed distinct compositional changes between fresh BE and SBE (Table 2). The oxygen content increased from 62.64% in BE to 67.90% in SBE, indicating that SBE retained more oxygenated organic residues derived from crude palm oil bleaching, such as oxidized fatty acids and triglycerides. In contrast, the relative proportions of Si and Al decreased (from 21.97 to 18.05% and from 4.45 to 4.11%, respectively), suggesting that the aluminosilicate framework of BE was partially covered by adsorbed organics, thereby lowering the detectable inorganic fraction [1].

In addition, Ca and K contents decreased after bleaching (from 4.99 to 3.29% and from 0.78 to 0.65%, respectively), which can be attributed to the formation of calcium and potassium soaps through reaction with free fatty acids in CPO. Interestingly, phosphorus appeared in SBE at 1.31%, which was absent in fresh BE, confirming the adsorption of phospholipids from the oil during the bleaching stage. Sulfur also decreased from 0.91% in BE to 0.49% in SBE, likely due to oxidative degradation of sulfur-containing organics.

Table 2. Elemental composition of BE and SBE determined by XRF (mass%)

Element	BE (mass%)	SBE (mass%)
O	62.640	67.900
Al	4.453	4.110
Si	21.974	18.050
P	-	1.305
S	0.912	0.499
K	0.783	0.651
Ca	4.994	3.290
Ti	0.591	0.548
Cr	0.019	0.018
Mn	0.041	0.038
Fe	3.531	3.533
Ni	0.016	0.016
Cu	0.014	0.014
Zn	0.007	0.009
Rb	0.005	0.005
Sr	0.014	0.010
Zr	0.011	0.007

Minor elements, such as Fe, Ti, Mn, Ni, Cu, Zn, Sr, Zr, Rb, and Cr, remained relatively stable, reflecting their natural presence in the clay matrix rather than contributions from oil. Overall, these results demonstrate that while the aluminosilicate backbone of BE remains intact, the bleaching process introduces substantial organic residues and modifies the distribution of alkali and alkaline earth metals in the spent adsorbent. These findings justify the need for thermal regeneration to remove organic contaminants. At the same time, the preserved aluminosilicate framework indicates that the material can be further modified through KOH impregnation to enhance its structural and morphological properties.

The Influence of SBE Treatment

Table 3 demonstrates the mass shifting of SBE in different stage procedures. The initial preparation step (hot water washing and filtration) reduced the mass from 100 to 93.60 g, primarily due to the removal of oil residues, soluble organics, and loosely attached impurities [14]. Calcination at 586 °C further decreased the mass drastically to 54.51 g. This reduction is attributed to the evaporation of physically adsorbed water, decomposition of residual triglycerides, phospholipids, and carbonaceous matter, as well as dehydroxylation of the clay structure [19]. As a result, the surface area and porosity of SBE are enhanced [20], providing a cleaner and more active matrix for further impregnation. This explains the significant mass reduction observed at this stage (54.51%), as also reported in similar regeneration studies [21].

Table 3. The alteration of the SBE mass in several regeneration processes

Sample	Mass (g)
SBE	100.00
SBE-Preparation	93.60
SBE-T	54.51
K-SBE-1	43.47
K-SBE-0.1	44.99
K-SBE-0.01	43.28

Impregnation with KOH may induce further dissolution and leaching of residual organics and weakly bound inorganic salts (e.g., phosphates, Ca^{2+}, Mg^{2+}, and other trace metals from crude oil refining) [19]. Consequently, the regenerated SBE mass primarily reflects the mineral matrix of bentonite/montmorillonite with enhanced alkalinity after KOH loading [22]. This indicates that calcination removes oil residues, volatile matter, and blocks in the pore structure, thereby facilitating more effective KOH impregnation. In this study, three different KOH concentrations (1.00, 0.10, and 0.01 M) were applied. The impregnation process reduced SBE mass by up to ~10% relative to calcined SBE, with the 0.1 M KOH treatment yielding the highest retained mass after impregnation. This trend indicates that the KOH concentration affects the balance between leaching and KOH uptake during regeneration.

Considering the color change observed in Fig. 1, SBE appears as a dark-brown wet powder due to the presence of oil, pigments, phospholipids, and other carbonaceous residues [23] from the bleaching process of CPO. During calcination at 500 °C, these organic compounds are oxidized or volatilized [16,24], leaving behind the mineral matrix with a lighter reddish-brown hue. The reddish tint after calcination and impregnation is likely associated with oxide species present in SBE [25]. Subsequent KOH impregnation at different concentrations did not alter the color, as the major chromophoric impurities had already

Fig 1. Visualization of (a) SBE, (b) SBE-T, (c) K-SBE-1, (d) K-SBE-0.1, (e) K-SBE-0.01, and (f) BE

been removed during calcination. Additionally, KOH itself is colorless, affecting only the surface chemistry without producing new colored species. In contrast, commercial activated bleaching earth typically exhibits a pale-white color, highlighting the difference between regenerated and freshly activated materials.

Characterization

Scanning electron microscope

SEM analysis is employed to ascertain the microstructure of a material, encompassing its texture, morphology, content, and details of particles. The elemental content on the surface of the catalyst material was determined using EDX. This analysis revealed the morphology of the particles, including their shape, size, and arrangement of SBE and its variant treatments. This analysis is performed at $10^4\times$ magnification. Fig. 2(a) illustrates that dirty SBE has the largest bulk size among all SBE types. It may be caused by dirt and oil trapped in the SBE pores [26].

After calcination (Fig. 2(b)), the structure became more fragmented with visible voids, indicating removal of organics and dehydroxylation of the clay. Impregnation with 1 M KOH in Fig. 2(c) resulted in a relatively compact morphology, suggesting partial restructuring due to strong alkaline attack. In contrast, lower KOH concentrations (0.10 and 0.01 M; Fig. 2(d) and 2(e)) produced more open and spongy structures, reflecting moderate leaching and partial dealumination that enhanced pore accessibility. For comparison, BE in Fig. 2(f) shows a more uniform lamellar morphology, indicating that regeneration improved SBE structure but did not fully restore it to the original BE state.

All three KOH concentrations resulted in SBE with similarly small bulk size, suggesting that variation in KOH concentration did not significantly influence overall particle dimensions. However, differences were more evident in surface morphology rather than bulk size. The bulk size of the original BE was larger than that of the KOH-impregnated SBE, which was closer to the calcined SBE but still smaller than the untreated SBE. This reduction indicates that both calcination and alkaline soaking contributed to particle disintegration—calcination through thermal stress and dehydroxylation, and alkaline soaking through chemical etching of the aluminosilicate framework [20].

By creating new spaces between particles and reducing particle aggregation, the impregnation of SBE with KOH (K-SBE) can enhance the specific surface area. SEM images reveal that the SBE surfaces become more porous and fragmented after KOH treatment, indicating structural modification. Although KOH cannot be directly identified from SEM alone, its incorporation is supported by EDX analysis, which revealed distinct potassium (K) peaks in the impregnated samples.

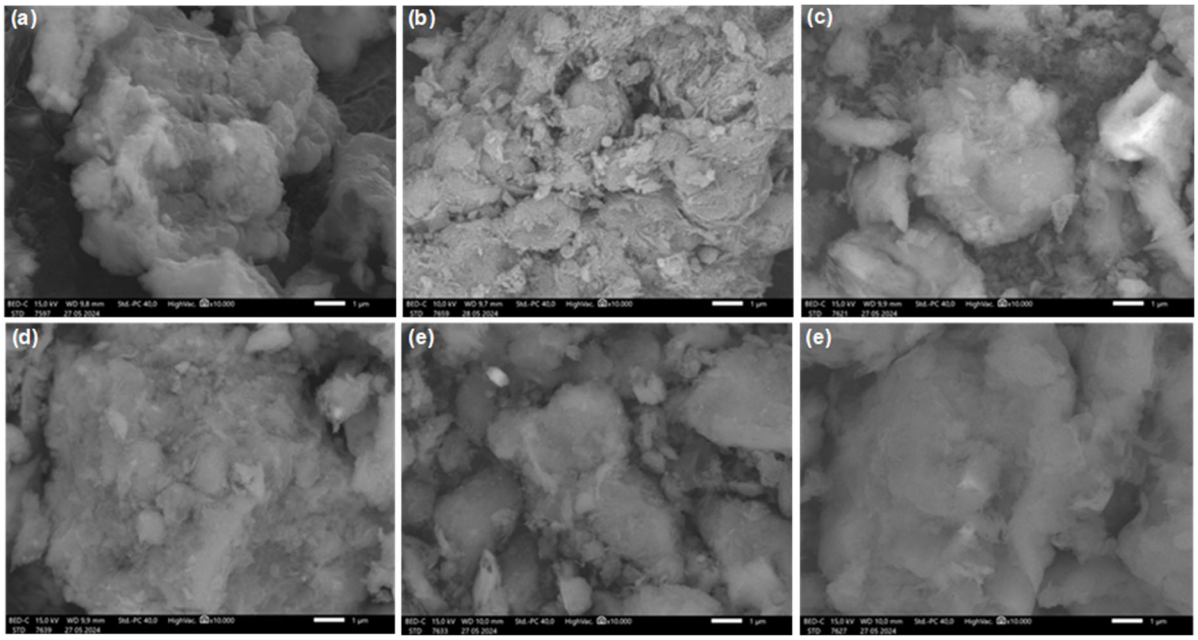

Fig 2. SEM Images in 1 μm of (a) SBE, (b) SBE-T, (c) K-SBE-1, (d) K-SBE-0.1, (e) K-SBE-0.01, and (f) BE

The SEM micrographs (Fig. 2) reveal significant morphological differences between raw SBE, regenerated SBE, and KOH-impregnated samples. Raw SBE shows dense agglomerates with limited visible porosity, attributed to pore blockage by residual organics. Calcination (SBE-T) partially restores pore accessibility, as indicated by a more open texture. Upon KOH impregnation, the surface becomes rougher and more fragmented, suggesting that alkaline treatment induces structural modifications that enhance porosity. Notably, the degree of morphological alteration correlates with KOH loading: K-SBE-1 exhibits extensive fragmentation, whereas K-SBE-0.01 retains a relatively compact structure. Compared to bleaching earth, which shows layered lamellar morphology, all SBE-derived samples demonstrate compaction and restructuring, confirming that regeneration and chemical activation significantly transform the clay matrix.

The structural changes seen in the SEM images are further supported by elemental analysis using EDX, which provides insight into the compositional changes of SBE during calcination and KOH impregnation. Fig. 3 and Table 4 display the EDX mapping results from the SEM analysis of SBE and its treatment. This is compared with BE. The EDX mapping technique reveals the many constituents within the adsorbents. The results indicate that the composition of SBE includes oxygen (O), silicon (Si), and aluminum (Al), suggesting that the main framework of the material is aluminosilicate, typical of montmorillonite-based bleaching earth. Minor elements, such as calcium (Ca) and magnesium (Mg), were also detected, likely originating from metallic impurities or soap residues formed during the bleaching process. The elemental makeup of SBE samples varies depending on the treatment applied.

Elemental composition analysis by SEM-EDX (Fig. 3 and Table 4) revealed that the elemental composition of SBE and its regenerated forms changed depending on the treatment applied. After calcination (SBE-T), the relative content of Al and Si slightly increased compared to untreated SBE, which indicates the removal of volatile organic matter and carbonaceous residues, leaving behind the aluminosilicate framework [1]. The oxygen content also increased, consistent with the dehydroxylation and oxidation processes that occur during heating. Upon KOH impregnation, K was successfully introduced into the structure, as evidenced by its clear appearance in K-SBE samples, indicating surface modification and possible ion exchange with Ca and Mg. Indeed, a decrease in Ca and Mg was observed

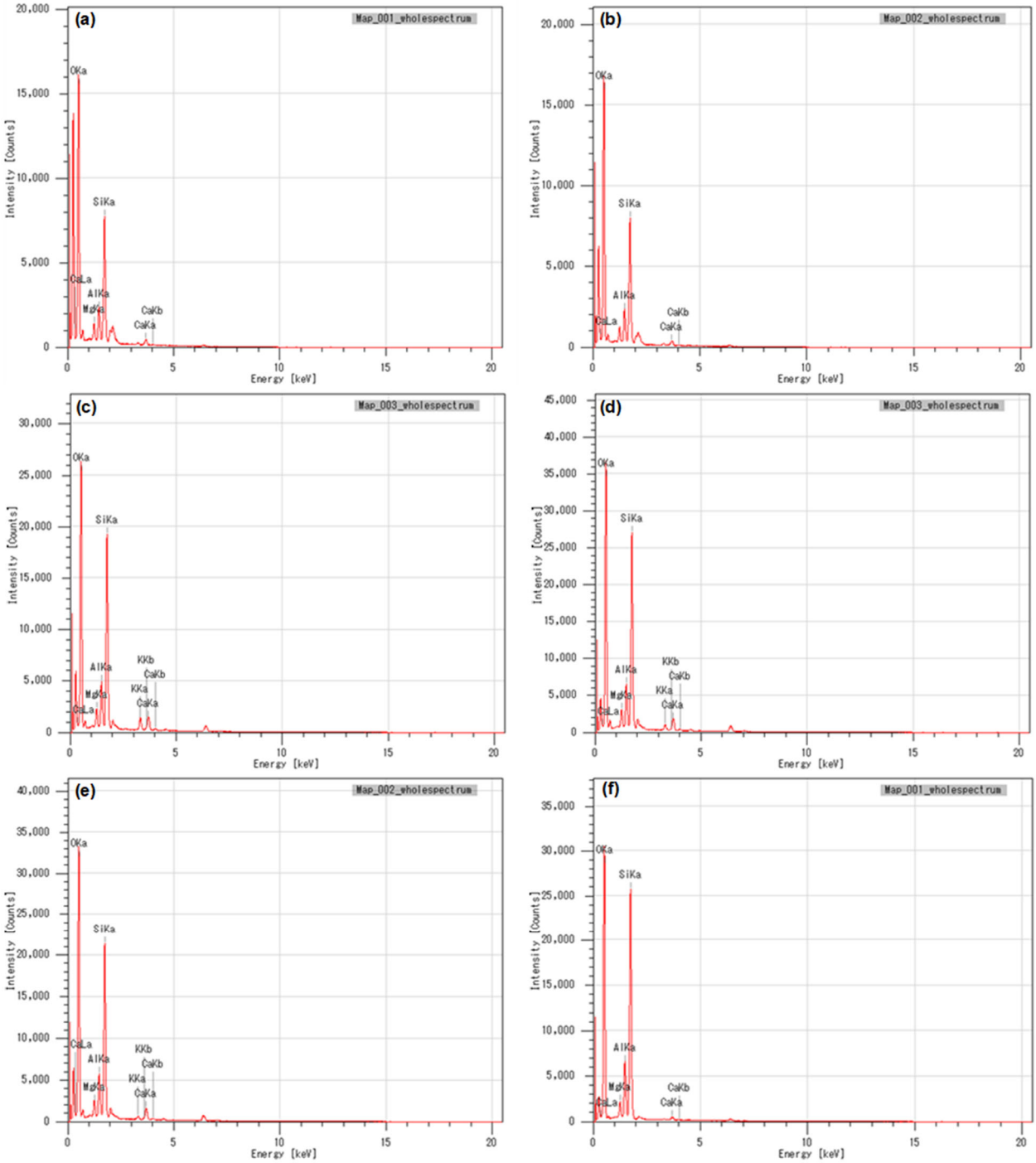

Fig 3. Distribution of elements in (a) SBE, (b) SBE-T, (c) K-SBE-1, (d) K-SBE-0.1, (e) K-SBE-0.01, and (f) BE

after KOH treatment, which may result from partial leaching or substitution by K^+ ions. The proportion of Si fluctuated depending on the KOH concentration, with a tendency toward higher values at moderate impregnation, which reflects partial structural rearrangement of the silicate matrix [19]. Overall, these changes demonstrate that calcination primarily removes organics and enriches the aluminosilicate backbone, while KOH impregnation incorporates potassium and modifies the surface chemistry through cation exchange and framework alteration. Upon KOH impregnation, a new element, K, appears in all K-SBE samples, confirming

Table 4. The quantities of SBE and each treatment compared to BE

Element	SBE		SBE-T		K-SBE 1N		K-SBE-0.1		K-SBE-0.01		BE	
	Mass (%)	Atom (%)	Mass (%)	Atom (%)	Mass (%)	Atom (%)	Mass (%)	Atom (%)	Mass (%)	Atom (%)	Mass (%)	Atom (%)
Al	6.86	5.03	7.16	5.20	5.69	7.61	5.54	4.15	5.93	4.30	6.04	4.33
Ca	4.21	2.08	4.12	2.02	4.44	1.03	0.50	2.18	4.07	1.99	4.01	1.93
K	-	-	-	-	3.29	-	-	1.66	1.58	0.79	0.93	0.46
Mg	3.21	2.61	-	-	2.35	2.17	1.75	1.90	2.42	1.95	2.30	1.82
O	56.40	69.66	58.59	71.76	58.90	56.36	69.23	72.39	58.82	72.01	61.18	73.89
Si	29.31	20.62	30.12	21.02	25.32	32.84	22.98	17.73	27.18	18.95	25.54	17.57
Total	100	100	100	100	100	100	100	100	100	100	100	100

successful incorporation of KOH. The potassium content increases with KOH concentration, from 0.93% (mass) at 0.01 M to 3.29% at 1 M, indicating dose-dependent uptake. Notably, the oxygen content decreases slightly in the K-SBE-1 sample, which may be attributed to surface coverage or partial neutralization during impregnation.

Aluminum and silicon contents also shift subtly depending on the treatment. For instance, K-SBE 1 M shows a decrease in Si (25.32%) and Al (5.69%) compared to SBE-T, potentially due to surface masking by the impregnated KOH layer. Meanwhile, the Ca content in K-SBE-0.1 drops to 0.50%, possibly due to leaching during the impregnation and washing process. In untreated SBE, Ca is 4.21%, which slightly decreases after calcination to 4.12%. This suggests that Ca-containing compounds are thermally stable under the applied temperature [27]. However, a sharp drop is observed in the K-SBE-0.1 sample (0.50% mass), likely due to partial leaching or displacement by K^+ ions during the KOH impregnation and subsequent acid washing. The increasing Ca content in K-SBE-0.01 and K-SBE-1 samples suggests a concentration-dependent interaction where high or low KOH concentrations may not disrupt calcium as effectively as moderate concentrations.

Oxygen (O) is the most abundant element in all samples, consistent with the oxide-based nature of the material (e.g., SiO_2, Al_2O_3, MgO) [28]. The atomic O content increases slightly after calcination (from 69.66% in SBE to 71.76% in SBE-T), possibly due to surface dehydration and transformation of hydroxyl groups [29]. After KOH treatment, O content varies but generally stays between 56–72%, influenced by the formation or removal of surface hydroxyls, carbonate groups, or metal-oxygen bonds [30]. The relatively lower O percentage in the K-SBE-1 sample (56.36%) may indicate partial surface coverage or masking by KOH residues.

Transmission electron microscope

According to the TEM analysis, there are some differences between the BE, SBE, and regeneration treatments. BE appears as a dark spot, but in SBE, it is dominated by a light area. The dark spot occurs in SBE during thermal treatment, but when the treatment continues with impregnation using KOH, the dark area becomes lighter. The TEM micrographs (Fig. 4) clearly demonstrate the morphological evolution of BE following bleaching and regeneration treatments. BE (Fig. 4(f)) displays compact and darker regions, corresponding to the dense stacking of aluminosilicate lamellae and higher electron density in thicker particles. After being used in the crude palm oil bleaching process (Fig. 4(a)), the structure of SBE becomes more irregular and fragmented. This disordered morphology likely arises from pore blockage by adsorbed organic residues, such as pigments and triglycerides, as well as mechanical stress during oil adsorption and subsequent handling, which promotes partial aggregation and collapse of the layered structure.

Calcination at 586 °C (Fig. 4(b)) induces further microstructural modification. The presence of darker agglomerated regions suggests localized sintering and densification, consistent with thermal removal of volatiles and partial dehydroxylation of the clay framework. This process enhances structural integrity but may temporarily reduce surface accessibility. After KOH impregnation,

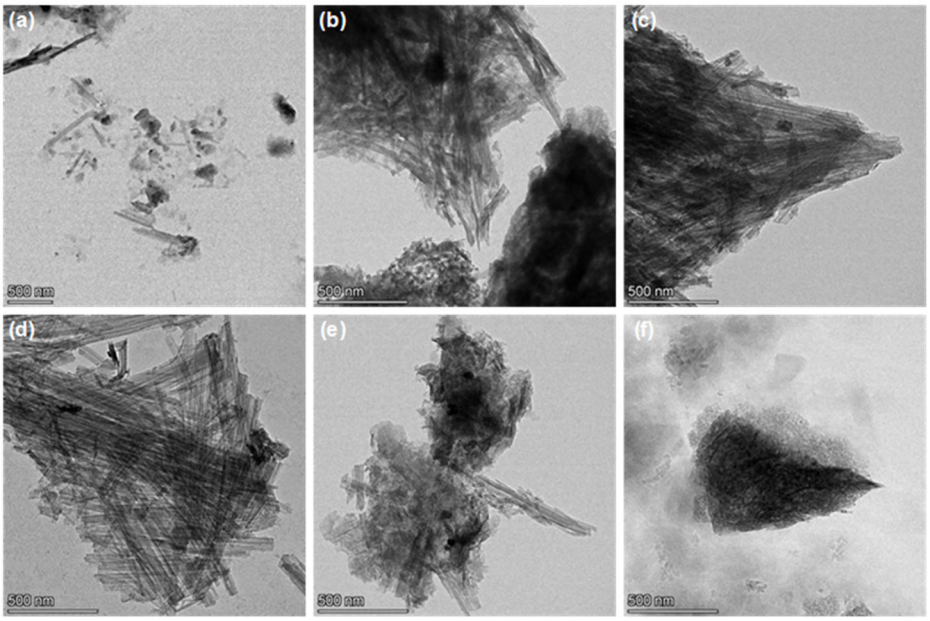

Fig 4. TEM images of (a) SBE, (b) SBE-T, (c) K-SBE-1, (d) K-SBE-0.1, (e) K-SBE-0.01, and (f) BE

however, the morphology becomes distinctly more heterogeneous. In the K-SBE-1 sample (Fig. 4(c)), brighter and more open regions are evident, indicating that strong alkaline conditions promote partial exfoliation and chemical etching of the aluminosilicate layers. In contrast, samples treated with lower KOH concentrations (0.10 and 0.01 M; Fig. 4(d) and 4(e)) show finer and more porous textures, reflecting moderate leaching and structural activation of the SBE matrix.

Overall, the TEM observations reveal a progressive transformation from compact lamellar structures in BE to more fragmented and porous networks in regenerated SBE, particularly after KOH treatment. Lower concentrations of KOH (0.10 and 0.01 M; Fig. 4(d) and 4(e)) produce even more open and dispersed morphologies, with brighter and less compact regions indicating enhanced porosity and lower electron density. These changes suggest partial delamination and chemical activation of the aluminosilicate layers. Such microstructural modifications facilitate greater surface exposure and pore accessibility, which are beneficial for adsorption and catalytic applications. While quantitative image analysis (e.g., particle size distribution) was not performed, the qualitative morphological changes observed by TEM are consistent with the increase in surface area and pore volume confirmed by BET analysis, demonstrating that both thermal and alkaline treatments synergistically enhance the textural properties of SBE.

X-ray diffraction

XRD analysis was performed to identify the crystalline phases of BE, SBE, SBE-T, and K-SBE samples. The diffractograms (Fig. 5) reveal differences in peak intensity and crystallinity among treatments, indicating structural modifications induced by calcination and KOH impregnation. Diffraction patterns of SBE, SBE-T, K-SBE-1, K-SBE-0.1, K-SBE-0.01, and BE

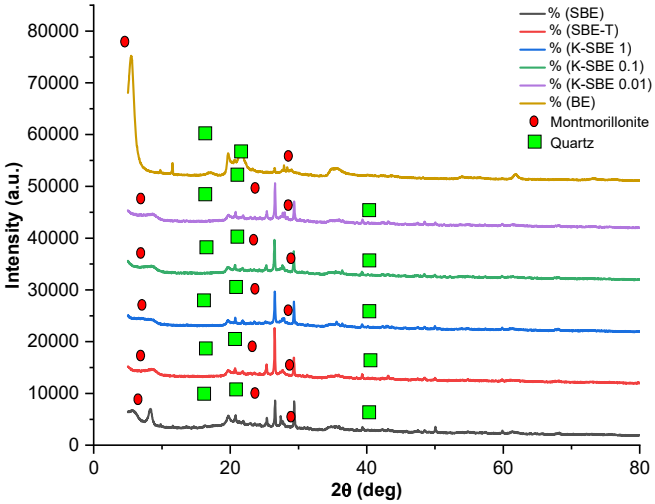

Fig 5. XRD of SBE and others compared to BE

samples can be seen in Fig. 5, showing that the diffractogram displayed a weak crystalline phase, as indicated by the observance of a relatively broad peak. SBE peaks are observed with 2θ on 8.3°, 20.8°, 25.3°, 26.6°, 29.4°, 35.6°, and 50.1°. In addition, the diffraction peaks are identical to those of quartz and montmorillonite [31-33]. In addition, the diffraction peaks are identical to the characteristics of quartz and montmorillonite. This could be because SBE and BE are derived from clays that contain many of these two components.

The peak intensity of the tested adsorbent showed a slight difference in comparison between SBE, SBE-T, and impregnated SBE. Raw SBE exhibited broader and less intense peaks, consistent with its partially amorphous structure caused by the presence of residual organics and oil-derived compounds. After calcination (SBE-T), the peaks became sharper and more intense, indicating the removal of volatile impurities and the enhancement of crystalline phases, such as quartz and montmorillonite. Upon KOH impregnation, the peak intensities varied depending on the concentration of KOH used. This variation is attributed to cation exchange of K^+ with Ca^{2+} and Mg^{2+}, partial dealumination of the clay framework, and possible incorporation of potassium into the silicate structure. Consequently, impregnation did not restore the crystallinity to the same degree as calcination but instead induced structural modifications that are reflected in the altered peak intensities.

Fig. 5, on the BE diffractogram, shows a different pattern, where the peak formed appears wider, indicating that the crystallinity index is lower than that of SBE. In general, BE is expected to exhibit a higher crystallinity index compared to SBE, since the bleaching process typically introduces residual organics and structural disorder. However, in Fig. 5, the BE sample exhibited broader peaks compared to SBE. This apparent discrepancy may be explained by the intrinsic properties of the commercial BE used in this study, which is acid-activated and contains a significant proportion of amorphous silica and alumina phases, thereby reducing its apparent crystallinity [34]. In contrast, calcination of SBE at elevated temperature removed volatile organic matter, carbonaceous residues, and adsorbed moisture, which may have enhanced the ordering of crystalline phases such as quartz and montmorillonite, leading to sharper peaks in the diffractogram [35]. Thus, the seemingly higher crystallinity in SBE relative to BE may not reflect a true structural improvement, but rather a combination of removal of amorphous fractions and enhanced detection of residual crystalline domains after regeneration. There was a slight difference in intensity, but no significant 2θ shift in the diffractogram generated from the XRD analysis.

EDX analysis (Table 4) reveals that the material is primarily composed of O, Si, and Al, with minor amounts of Ca, Mg, and Fe, consistent with an aluminosilicate clay matrix. XRD diffractograms display a prominent reflection near 2θ≈26.6° (assigned to quartz, SiO_2) and low-angle features corresponding to layered smectite/montmorillonite-type phases. TEM images reveal lamellar sheet morphology for fresh BE and increased fragmentation for SBE after use. Taken together, these data indicate that SBE consists of a montmorillonite-like aluminosilicate framework (Si–O–Al backbone) whose surface and pores are substantially masked by adsorbed oil-derived organics (triglycerides, phospholipids) and associated metallic soaps (Ca/Mg salts). EDX detects potassium after KOH treatment, but the absence of distinct K-phase peaks in XRD suggests that K is incorporated mainly by surface dispersion or ion exchange rather than forming a crystalline potassium compound.

Surface area, pore volume, and pore size analysis

Surface area and adsorbent porosity measurements were carried out using BET. The SAA was used to carry out the surface area analysis. The BJH equation was used to calculate the distribution of pore size, and the value of the pore volume at p/p_0 ~1 was used to calculate the volume of the entire pore [18]. Table 5 presents the values of surface area, pore volume, and pore size for SBE under different treatments. Dirty SBE has the lowest surface area, pore volume, and pore size. It indicates that other materials had covered the pore of SBE within bleaching processes, such as impurities (chlorophylls, carotenes, hydroperoxides, free fatty acids, and non-glyceride substances that are absorbed from crude edible oil) [23].

Table 5. Specific surface areas and pore properties of SBE and its treatments compared to BE

Sample	Surface area ($m^2\ g^{-1}$)	Pore volume ($cc\ g^{-1}$)	Pore size (Å)
SBE	8.70	0.0180	14.48
SBE T	84.54	0.2233	18.97
K-SBE-1	80.69	0.2081	18.97
K-SBE-0.1	93.81	0.2249	18.97
K-SBE-0.01	88.61	0.2221	18.97
BE	94.29	0.2188	18.97

After SBE had been calcined at 586 °C for 108 min, the surface area of SBE greatly increased up to ten times compared to dirty SBE, because the purpose of heating is to remove impurities or other organics. Calcination affects both volume and pore size; it can enlarge the pore and shrink the pore volume [36]. The pore volume increases 100× over the filthy SBE, while the pore size grows to 18.97 Å. The pore size indicates the pore diameter of SBE. This study presents that the pore size of SBE can be enlarged by thermal treatment. The increase in pore size from 14.48 (SBE) to 18.97 Å (SBE-T) is attributed to the calcination process, which removes residual organics, moisture, and oil-derived impurities that block the clay pores [37]. High-temperature treatment also induces dehydroxylation of the clay surface, leading to structural rearrangements that open pore channels and enlarge pore diameters. In contrast, subsequent KOH impregnation did not significantly alter the pore size (remaining ~18.97 Å across all concentrations), as the alkaline treatment mainly modifies surface chemistry and introduces potassium species through ion exchange or deposition, without drastically changing the overall pore framework. This suggests that calcination is the primary step in optimizing SBE pore size, while KOH impregnation primarily affects surface composition and surface area, rather than pore diameter.

Particle agglomeration was decreased, and new gaps were created between particles when KOH was impregnated on SBE. This occurs because the alkaline solution partially dissolves amorphous silica and leaches exchangeable cations (e.g., Ca^{2+}, Mg^{2+}) from the aluminosilicate matrix. Such chemical etching weakens the inter-particle bonds and disintegrates large aggregates into smaller fragments. Additionally, K^+ ions introduced during impregnation can replace native cations in the clay framework through ion exchange, thereby further disrupting particle cohesion. These combined effects reduce particle agglomeration [38], generate inter-particle voids, and consequently increase the accessible surface area of the material [39].

Heating at high temperatures can evaporate the oil content of the SBE [40]. However, the surface area of calcined SBE does not match that of BE. KOH impregnation increases the surface area of SBE. The test findings reveal that impregnation with 0.1 M KOH yields a surface area similar to BE, relatively. This number is further corroborated by the fact that SBE impregnated with 0.1 M KOH has a greater pore volume than BE with the same pore size. Data suggests that impregnating SBE with KOH after calcination can improve its porosity and surface area. However, increasing the concentration of KOH reduces the surface area and pore volume of SBE. This is because impregnation can block pores, lowering the adsorption capacity [41]. To improve SBE porosity and surface area, the concentration of KOH during impregnation must be carefully controlled.

The N_2 adsorption–desorption isotherms of SBE, SBE-T, K-SBE, and BE (Fig. 6) exhibit Type IV curves with H3 type hysteresis loops, indicating that all materials possess mesoporous structures dominated by slit-shaped pores typical of layered aluminosilicate clays such as montmorillonite. The SBE sample exhibits the lowest nitrogen uptake due to pore blockage by residual organic compounds accumulated during the bleaching process. In contrast, SBE-T demonstrates a substantial increase in adsorption capacity, confirming that thermal treatment effectively removes volatile organics and reopens the blocked pores. This treatment enhances both surface and pore volume, consistent with the finding of pre-reopening upon thermal regeneration [20].

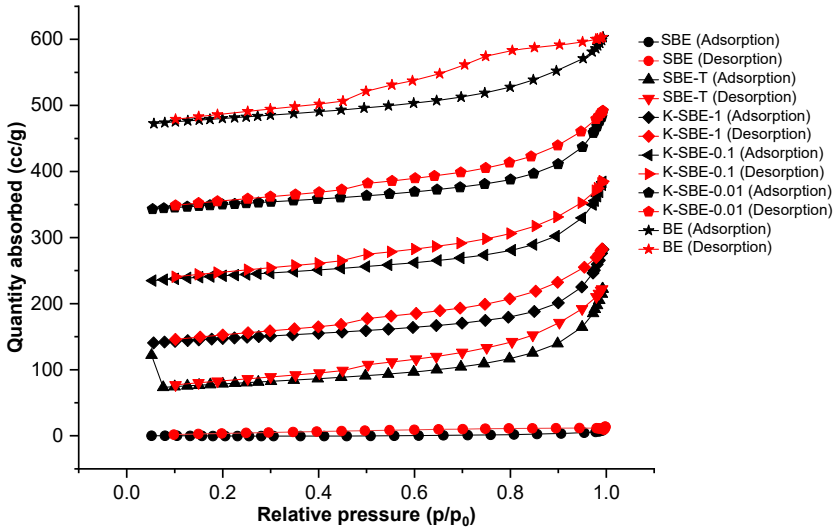

Fig 6. Adsorption–desorption isotherms of SBE and its regenerated variants compared to BE

Upon KOH impregnation, the isotherm profiles vary depending on alkali concentration: K-SBE-0.1 exhibits the highest nitrogen adsorption, suggesting optimal surface activation and partial delamination, while K-SBE-1 shows a slightly reduced uptake, possibly caused by over-dealumination or partial pore collapse at higher alkalinity. At low relative pressures ($p/p_0 < 0.1$), all samples show monolayer adsorption on micropores, followed by capillary condensation in the mesopore range ($p/p_0 > 0.4$), confirming the coexistence of microporous and mesoporous structures. These results demonstrate that the combined thermal and alkaline treatments promote structural reorganization, enhance porosity, and improve surface accessibility, making regenerated SBE more suitable for catalytic and adsorption applications.

■ CONCLUSION

The results of this study showed that SBE regeneration by using KOH impregnation improves the morphological structure of SBE. Impregnation can reduce the particle size of SBE. In surface area analysis, optimum regeneration is achieved by impregnating with 0.1 M KOH. This variation has the most similar surface area number to pure BE and has greater pore volume. Furthermore, it can be concluded that SBE regeneration using thermal treatment and subsequent 0.1 M KOH impregnation has the optimal scale for regenerating SBE.

■ ACKNOWLEDGMENTS

The researchers gratefully acknowledge the Ministry of Education, Culture, Research, and Technology of Indonesia by the research grant number 88/SPK/D.D4/PPK.01.APTV/III/2024 for its funding support of this study, and the Directorate of Research and Development Talent, Directorate General of Research and Development, for their valuable assistance in the preparation of this international publication.

■ CONFLICT OF INTEREST

The authors declare that they have no conflicts of interest.

■ AUTHOR CONTRIBUTIONS

Ika Kusuma Nugraheni and Sunardi proposed the concept. Putri Iis Faiza conducted the experiments, while Dita Adi Saputra performed the sample analysis at the BRIN laboratory. Utami Irawati, Ika Kusuma Nugraheni, Jaka Darma Jaya, and Nuryati discussed the laboratory results. Ika Kusuma Nugraheni and Jaka Darma Jaya wrote the manuscript. All authors read and approved the final version of the manuscript.

■ REFERENCES

[1] Abdelbasir, S.M., Shehab, A.I., and Khalek, M.A.A., 2023, Spent bleaching earth; recycling and

utilization techniques: A review, *Resour., Conserv. Recyl. Adv.*, 17, 200124.

[2] Shahi, M., Sabour, M.R., Amiri, A., and Ghasemnezhad, M., 2015, Cleaning spent bleaching clay through using solvent extraction method and RSM statistical approach, *Cumhuriyet Sci. J.*, 36 (7), 23–40.

[3] Maharani, D.R., Ruhiyat, R., Iswanto, B., and Juliani, A., 2023, The use of spent bleaching earth (SBE) as an adsorbent to reduce free fatty acids in waste cooking oil, *Indones. J. Urban Environ. Technol.*, 5 (2), 193–208.

[4] Wangrakdiskul, U., Khonkaew, P., and Wongchareonsin, T., 2015, Use of the spent bleaching earth from palm oil industry in non fired wall tiles, *Int. J. Adv. Cult. Technol.*, 3 (2), 15–24.

[5] Yulikasari, A., Nurhayati, E., Utama, W., and Warmadewanthi, I., 2022, Characterization of spent bleaching earth as an adsorbent material for dye removal, *J. Ecol. Eng.*, 23 (4), 96–104.

[6] Zhang, C., Yu, M., Li, X., Li, X., Siyal, A.A., Liu, Y., Jin, Y., Dai, J., Wang, L., Zhou, C., Zhang, Y., Yuan, Y., Qu, J., Yu, H., Fu, J., Liu, C., and Li, Y., 2022, Disposal, regeneration and pyrolysis products characterization of spent bleaching clay from vegetable oil refinery in a fluidized bed pyrolyser, *J. Cleaner Prod.*, 346, 131157.

[7] Asmoro, P.D.R., Yuliana, M., Soetaredjo, F.E., Ismadji, S., Muraoka, M., Kawano, S., Shizuma, M., Kadja, G.T.M., Wijaya, C.J., Santoso, S.P., and Retnoningtyas, E.S., 2024, Efficient and selective phosphate removal from wastewater using surface-modified spent bleaching earth from palm oil refineries: A zero-waste approach, *J. Water Process Eng.*, 58, 104906.

[8] Handoko, O.T., Hasanudin, U., Suroso, E., Dermiyati, D., Yuwono, S.D., Ginting, S.B., Sugiharto, R., Indraningtyas, L., Amelia, J.R., and Iryani, D.A., 2024, Economic and environmental analysis of spent bleaching earth reactivation, *IOP Conf. Ser.: Earth Environ. Sci.*, 1308 (1), 012061.

[9] Loh, S.K., James, S., Ngatiman, M., Cheong, K.Y., Choo, Y.M., and Lim, W.S., 2013, Enhancement of palm oil refinery waste – Spent bleaching earth (SBE) into bio organic fertilizer and their effects on crop biomass growth, *Ind. Crops Prod.*, 49, 775–781.

[10] Sunartono, S., Lenggogeni, L., Handayani, I.D., Setiawan, H., Adiarso, A., Nelly, A., Hermawan, A., Wijono, R.A., Wicaksana, D.E.P., Marsudi, A., Setiyadi, E.D., Saparudin, S., Setiadi, S., Ferabianie, A.L., and Dewi, Y.R., 2025, Assessing competitiveness and sustainability of the cooking oil industry through the valuation of eco-efficiency on the utilization of spent bleaching earth, *Case Stud. Chem. Environ. Eng.*, 11, 101176.

[11] Boukerroui, A., and Ouali, M.S., 2020, Regeneration of a spent bleaching earth and its reuse in the refining of an edible oil, *J. Chem. Technol. Biotechnol.*, 75 (9), 773–776.

[12] Khan, A., 2015, Bleaching of vegetable oil using organic acid activated fuller's earth (bentonite clay), *Global J. Res. Eng., C*, 15 (C2), 1–6.

[13] Oladosu, W.A., Manan, Z.A., and Wan Alwi, S.R., 2017, Recovery of vegetable oil from spent bleaching earth: State-of-the-art and prospect for process intensification, *Chem. Eng. Trans.*, 56, 133–138.

[14] Bachmann, S.A.L., Valle, R.C.S.C., Vegini, A.A., and Tavares, L.B.B., 2020, Determination of optimum conditions for thermal regeneration and characterization of a spent bleaching earth, *J. Environ. Chem. Eng.*, 8 (2), 103503.

[15] Tsai, W.T., and Lai, C.W., 2006, Adsorption of herbicide paraquat by clay mineral regenerated from spent bleaching earth, *J. Hazard. Mater.*, 134 (1), 144–148.

[16] Nguemtchouin Mbouga, M.G., Ngassoum, M.B., Kamga, R., and Cretin, M., 2018, Characterization of acidic and alkali treated kaolinite and montmorillonite clay from Adamawa and far-north region of Cameroon, *J. Appl. Chem. Sci. Int.*, 9 (1), 26–38.

[17] Saviola, A.J., Wijaya, K., Syoufian, A., Saputri, W.D., Saputra, D.A., Aziz, I.T.A., and Oh, W.C., 2024, Hydroconversion of used palm cooking oil into bio-jet fuel over phosphoric acid-modified

nano-zirconia catalyst, *Case Stud. Chem. Environ. Eng.*, 9, 100653.

[18] Saputra, D.A., Amin, A.K., Wijaya, K., Triyono, T., Trisunaryanti, W., Fitroturokhmah, A., and Oh, W.C., 2024, MgO/γ-Alumina and CaO/γ-alumina catalysts for the transesterification of castor oil (*Ricinus communis*) into biodiesel, *Iran. J. Chem. Chem. Eng.*, 43 (4), 1622–1634.

[19] Borno, I.B., and Ashraf, W., 2023, Effects of co-calcining kaolinite-rich clay blends with alkali and alkali earth metal hydroxides, *Appl. Clay Sci.*, 231, 106742.

[20] Liu, W., Yuan, K., Yin, K., Zuo, S., and Yao, C., 2020, Clay-activated carbon adsorbent obtained by activation of spent bleaching earth and its application for removing Pb(II) ion, *Environ. Sci. Pollut. Res.*, 28 (1), 711–723.

[21] Keasavan, T., Loh, S.K., Jaafar, N.F., Rahmawati, Z., and Wan Abdullah, W.N., 2023, Synthesis of biodiesel from residual oil extracted from spent bleaching earth using spent bleaching earth-supported catalyst, *Chem. Eng. Res. Des.*, 200, 716–728.

[22] Wu, G., Liu, S., Chen, Z., Yu, Q., Chu, Y., Xiao, H., Peng, H., Fang, D., Deng, S., and Chen, Y., 2022, Promotion effect of alkaline leaching on the catalytic performance over Cu/Fe-SSZ-13 catalyst for selective catalytic reduction of NO_x with NH_3, *J. Taiwan Inst. Chem. Eng.*, 134, 104355.

[23] Machmudah, S., Maulana, N.A., Norman, A.S.M., Nyoto, V.M., Amrullah, I., Wahyudiono, W., Winardi, S., Wenten, I.G., and Goto, M., 2022, Oil removal from spent bleaching earth of vegetable oil refinery plant using supercritical carbon dioxide, *Heliyon*, 8 (10), e10826.

[24] Moklis, M.H., Cheng, S., and Cross, J.S., 2023, Current and future trends for crude glycerol upgrading to high value-added products, *Sustainability*, 15 (4), 2979.

[25] Cheng, K., You, Q., Zou, L., Zhang, Y., Wang, P., and Zhang, W., 2025, High-temperature calcination modified red clay as an efficient adsorbent for phosphate removal from water, *Environ. Res.*, 268, 120704.

[26] Yenie, E., Bahri, S., Hapsoh, H., and Saputra, E., 2023, Synthesis of composite adsorbent based on spent mushroom substrate (SMS) and spent bleaching earth (SBE), *Mater. Today: Proc.*, 87, 93–100.

[27] Igami, R., Igarashi, G., Aili, A., Minato, D., Kurihara, R., and Maruyama, I., 2025, Clinker mineral formation and thermal decomposition of calcium carbonates in carbonated tobermorites: Mechanism of CO_2 release in low-temperature ranges, *Cem. Concr. Res.*, 197, 107969.

[28] Douglas-Song, T., Ota, T., Yamanaka, M., Kitagawa, H., Tanaka, R., Potiszil, C., and Kunihiro, T., 2025, Lithium- and oxygen-isotope compositions of a Si-rich nebular reservoir determined from chondrule constituents in the Sahara 97103 EH3 chondrite, *Geochim. Cosmochim. Acta*, 400, 51–71.

[29] Dhar, M., and Bishnoi, S., 2024, Influence of calcination temperature on the physical and chemical characteristics of kaolinitic clays for use as supplementary cementitious materials, *Cem. Concr. Res.*, 178, 107464.

[30] Qiu, C., Jiang, L., Gao, Y., and Sheng, L., 2023, Effects of oxygen-containing functional groups on carbon materials in supercapacitors: A review, *Mater. Des.*, 230, 111952.

[31] Saputra, E., Utama, P.S., Irdoni, H.S., Simatupang, M.D.V., Prawiranegara, B.A., Abid, H.R., and Muraza, O., 2020, Spent bleaching earth supported $CeFeO_3$ perovskite for visible light photocatalytic oxidation of methylene blue, *J. Appl. Mater. Technol.*, 1 (2), 81–87.

[32] Tang, J., Mu, B., Zheng, M., and Wang, A., 2015, One-step calcination of the spent bleaching earth for the efficient removal of heavy metal ions, *ACS Sustainable Chem. Eng.*, 3 (6), 1125–1135.

[33] Zhou, F., Liu, Q., Liu, X., Li, W., Feng, J., and Chi, R.A., 2020, Surface electrical behaviors of apatite, dolomite, quartz, and phosphate ore, *Front. Mater.*, 7, 35.

[34] Martirena Hernández, J.F., Antoni, M., Yanisleidy Oquendo-Machado, Y., Borrajo-Perez, R., Alujas-

Diaz, A., and Almenares-Reyes, R., 2023, Impact of calcination technology on properties of calcined clays, *RILEM Tech. Lett.*, 8, 190–197.

[35] Werling, N., Kaltenbach, J., Weidler, P.G., Schuhmann, R., Dehn, F., and Emmerich, K., 2022, Solubility of calcined kaolinite, montmorillonite, and illite in high molar NaOH and suitability as precursors for geopolymers, *Clays Clay Miner.*, 70 (2), 270–289.

[36] Takht Ravanchi, M., Rahimi Fard, M., Fadaeerayeni, S., and Yaripour, F., 2015, Effect of calcination conditions on crystalline structure and pore size distribution for a mesoporous alumina, *Chem. Eng. Commun.*, 202 (4), 493–499.

[37] Putri, S.E., Ahmad, A., Raya, I., Tjahjanto, R.T., Irfandi, R., Karim, H., Desa, S.S., and Rahman, A., 2023, The effect of thermal treatment on the characteristics of porous ceramic-based natural clay and chitosan biopolymer precursors, *Indones. J. Chem.*, 23 (3), 727–741.

[38] Li, Q., and Lueking, A.D., 2011, Effect of surface oxygen groups and water on hydrogen spillover in Pt-doped activated carbon, *J. Phys. Chem. C*, 115 (10), 4273–4282.

[39] Wijaya, K., Saviola, A.J., Amin, A.K., Vebryana, M.F., Bhagaskara, A., Ekawati, H.A., Ramadhani, S., Saputra, D.A., and Agustanhakri, A., 2024, Performance of hydrothermally prepared NiMo dispersed on sulfated zirconia nano-catalyst in the conversion of used palm cooking oil into jet fuel range bio-hydrocarbons, *Bull. Chem. React. Eng. Catal.*, 19 (2), 361–371.

[40] Zhuang, Y., Dong, J., He, X., Wang, J., Li, C., Dong, L., Zhang, Y., Zhou, X., Wang, H., Yi, Y., and Wang, S., 2022, Impact of heating temperature and fatty acid type on the formation of lipid oxidation products during thermal processing, *Front. Nutr.*, 9, 913297.

[41] Zakaria, R., Jamalluddin, N.A., and Abu Bakar, M.Z., 2021, Effect of impregnation ratio and activation temperature on the yield and adsorption performance of mangrove based activated carbon for methylene blue removal, *Results Mater.*, 10, 100183.